Journal of
Mechanics of Materials and Structures

SERRATION EFFECTS ON INTERFACIAL CRACKS

Assimina A. Pelegri and Baoxiang X. Shan

Volume 2, Nº 9 *November 2007*

mathematical sciences publishers

JOURNAL OF MECHANICS OF MATERIALS AND STRUCTURES
Vol. 2, No. 9, 2007

SERRATION EFFECTS ON INTERFACIAL CRACKS

ASSIMINA A. PELEGRI AND BAOXIANG X. SHAN

To investigate the effect of serrations in an interfacial crack between dissimilar materials, we introduce into the Finite Element (FE) framework a unit cell (UC) at microscale. By assigning material-specific properties to these unit cells, we can model various serration profiles and distributions and calculate their effect on the mixed-mode stress intensity factor (SIF), including its magnitude and phase angle. The simulation demonstrates that serration profoundly changes the local behavior of an interfacial crack. The serrations decrease the SIF in mode I, increase it in mode II, and, when the serration's height-to-width ratio increases, the mode mixity SIF increases as well. We find that sparse serration confines variation in the SIFs to the local peaks and that dense serrations cause widespread undulations in the SIF's magnitude and phase angle.

1. Introduction

Materials scientists are increasingly interested in fractures at the interface between two dissimilar materials, because they are fundamental for understanding thin-film coatings [Hutchinson and Suo 1992; Diao and Kato 1994; Mishnaevsky and Gross 2005], electronic packaging, adhesion [Straffelini 2001; Packham 2003], and composites and biomaterials [Wang and Agrawal 2000; Lucksanasombool et al. 2003]. Experiments cumulatively show that the waviness at the interface profoundly effects interfacial crack propagation. Liechti [2007] has made atomic force microscope (AFM) images of cracks at a glass/epoxy interface. Shown in Figure 1, they clearly demonstrate that the interfacial crack is not smooth and flat, but rather features dense sharp hackles and serrations. Hackles and serrations appear also in fractographic images of composites, such as Carbon/Fibredux-97 [Partridge and Singh 1995] and T300H/914C [Gilchrist and Svensson 1995; Gilchrist et al. 1996], especially in the mode II dominant conditions.

Previously, serrations and hackles were modeled by first identifying a scalar material parameter with the interfacial roughness and then investigating its effect on interfacial fracture and strength [Cao and Evans 1989; Ramulu et al. 2001; Lucksanasombool et al. 2003; Packham 2003]. Because the method is simple, it fails to capture micromechanical and microgeometric details at the interface and around the crack's tip. The FEM [Larson and Miles 1998; Schuller et al. 1999; Diao and Kandori 2006] and BEM [Young 2001] models adopt a more detailed view of the micromechanics. They represent the interfacial roughness by a discrete triangular arrangement of surface integral elements with specific period and amplitude. However, these models can accommodate only limited serration profiles and distributions.

Therefore, in the FEM framework, we introduce a specific unit cell (UC) so that we can more flexibly adjust the serration profile and distribution and hence investigate their effect on the magnitude and phase angle of the stress intensity factor.

Keywords: bimaterial, composites, interfacial crack, materials, mechanics, mixed mode, stress intensity factors, unit cells.

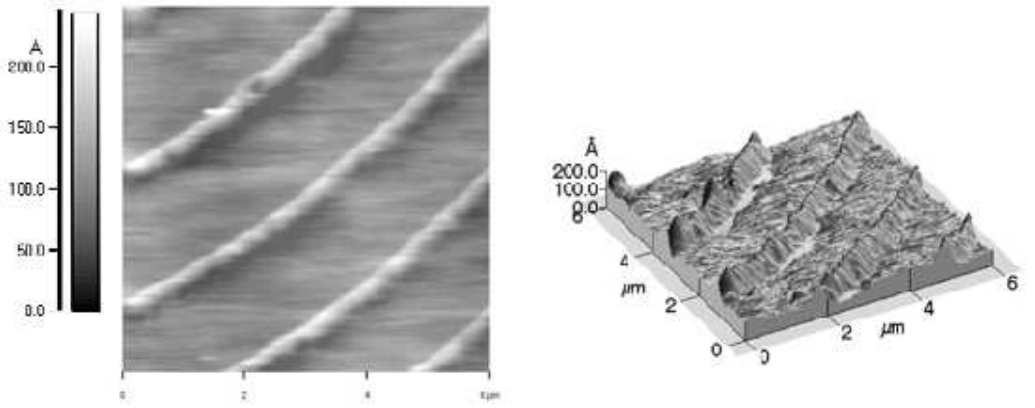

Figure 1. AFM images of a glass/epoxy interface crack.

2. Modeling

2.1. ***DCB sandwich specimen.*** In experiments, Lee and Qu [2003] investigated the effect of serration on interfacial adhesion using a double cantilever beam (DCB). We will use a similar setup to test the performance of our UC-based FE model. The specimen is shown in Figure 2, borrowed from [Lee and Qu 2003]: a leadframe sandwiches an epoxy molding component (EMC). Ours differs by setting the leadframe thickness to 1.7 mm, because we want to increase the initial phase angle shift. The global loads are opposite 200 N forces applied to the circle centers so as to open the crack further. To simulate the experimental setup, we set the structural boundary conditions as follows: the circle centers are free to move vertically, but are horizontally fixed. All edges are stress-free.

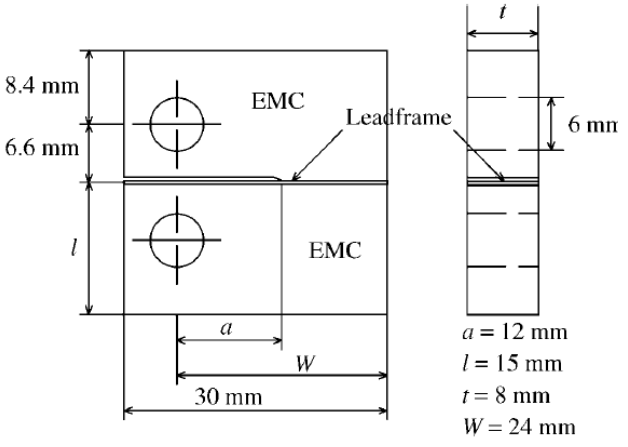

Figure 2. Geometry of DCB sandwich specimen.

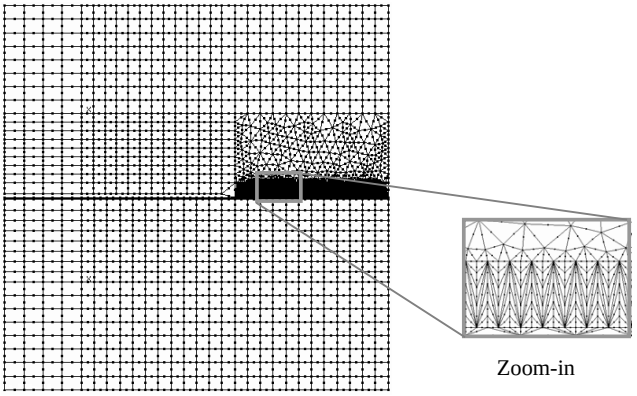

Figure 3. FEM elements of specimen.

The leadframe is a copper alloy, with Young's modulus $E = 127\,\text{GPa}$ and Poisson ratio $\nu = 0.34$. The EMC has Young's modulus $E = 3\,\text{GPa}$ and Poisson ratio $\nu = 0.3$.

2.2. ***FE model and unit cell.*** After we specify the DCB dimensions, we input them into CASCA, a 2-D mesh generator in the FE software package FRANC2DL [Swenson and James 1997]. We divided the specimen into several subregions to guarantee a fine mesh around the interface, especially at the crack tip and the potential crack trajectory. We allow the software to initially mesh the subregions, but, in the interface ahead of the crack tip, we fix the mesh manually, using our proposed unit cells. In addition to the surface boundary conditions, the interface is initially set to be perfectly binding before it cracks. After separation, the delaminated surfaces are free from any stress. The initial FE model of the sandwich specimen is shown in Figure 3, and the zoomed-in insert illustrates the meshing elements with specialized unit cells.

The FEM model was designed to explore the effect of serration on phase angle shift and specifically how different shapes and distributions affect the shift. We propose a general unit cell (UC) to avoid constructing a different FEM model each case. The unit cell, shown in Figure 4, has circular points numbered from 1–5 counterclockwise. For a unit cell whose height is six times its width, we list the slope angle for each marked point in Table 1.

Point	Height	Angle
1	$h/6$	45.0°
2	$h/3$	63.4°
3	$2h/3$	76.0°
4	h	80.5°
5	h	90.0°

Table 1. The height and angle of each point in UC.

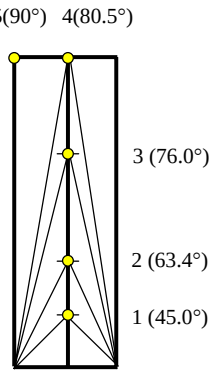

Figure 4. Unit cell for interfacial serration in FEM simulation.

Using the proposed unit cell, a number of serration patterns can be easily drawn and implemented in FEM. Each can be evolved from an initial FEM model by changing the expected cell from material 1 (EMC here) from material 2 (copper alloy here). Figure 5 demonstrates how the initial smooth and flat interface evolves into one with a pattern of small, sparse serrations.

After setting the profiles at the interface, we start the FE analysis for the crack tip at its initial position. Then, step by step, we simulate the progress of a growing crack by intentionally controlling the crack propagation direction and length in FRANC2DL. To ensure continued accuracy as the crack grows, finer analysis elements near the crack tip are generated automatically both inside and outside of the serration, as shown as Figure 6. We constrain the element size near the crack tip to be less than one quarter of the thin leadframe thickness, as this strikes a balance between good resolution and reasonable computation time [La Saponara et al. 2002].

2.3. ***Computation of stress intensity factors and mode mixity.*** In our FEM, we calculate the mode I and II stress intensity factors using the modified crack closure integral (MCCI) method [Rybicki and Kanninen 1977; Narayana and Dattaguru 1996; Sethuraman and Maiti 1988]. The method, first proposed by Rybicki and Kanninen [1977], was based on Irwin's virtual crack closure method. The principle of MCCI is that the energy to create a new crack surface is equal to the work required to close the crack

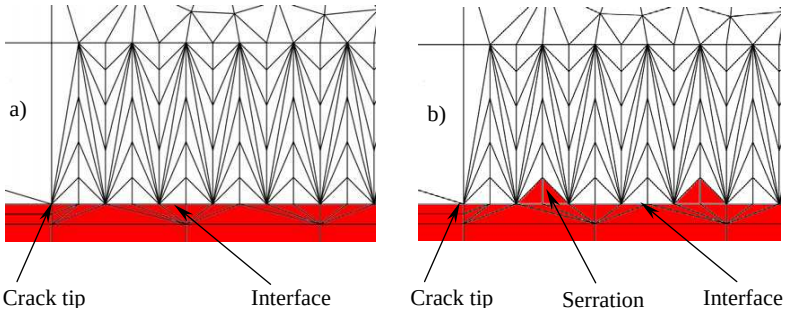

Figure 5. Evolution of FEM model: (a) initial FEM model without serration; (b) FEM model with sparse, small peaks.

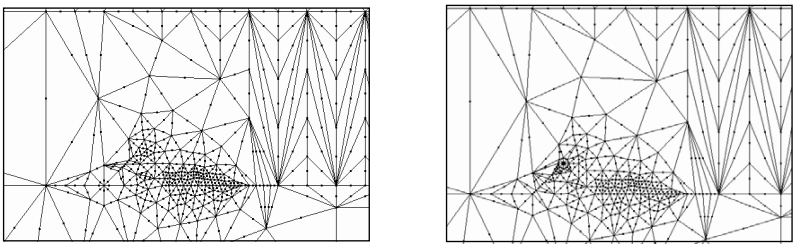

(a) (b)

Figure 6. Element refinement at the crack tip for the SIF computation: (a) finer elements around the crack tip at the serration's bottom corner; (b) finer elements around the crack tip at the serration's peak.

to its original length. The MCCI can calculate the strain energy release rates and stress intensity factors without assuming isotropy or homogeneity around a crack, and it calculates both the mode I and II stress intensity values in a single analysis. Hence this method is ideally suited for modeling interfacial cracks in bimaterials.

In MCCI, the strain energy release rates of modes I and II are [Kim and Paulino 2002]

$$G_I = \lim_{\delta a \to 0} \frac{2}{\delta a} \int_{x_1=0}^{x_1=\delta a} \frac{1}{2}\sigma_{22}(r = x_1, \theta = 0, a) \cdot u_2(r = \delta a - x_1, \theta = \pi, a + \delta a)\mathrm{d}x_1,$$

$$G_{II} = \lim_{\delta a \to 0} \frac{2}{\delta a} \int_{x_1=0}^{x_1=\delta a} \frac{1}{2}\sigma_{12}(r = x_1, \theta = 0, a) \cdot u_1(r = \delta a - x_1, \theta = \pi, a + \delta a)\mathrm{d}x_1,$$

where σ_{22} and σ_{12} are normal and shear stresses ahead of the crack tip, u_1 and u_2 are the relative displacements with respect to the crack tip, a is the length of initial crack, and δa is a virtual crack extension.

Raju [1987] expressed the two strain energy release rates in terms of the nodal forces and displacements by using six-node quarter-point triangular elements around the crack tip (see Figure 6), finding

$$\begin{aligned} G_I = \frac{1}{2\Delta a}\big[& F_{2,i}\big(t_{11}u_{2,i-2} + t_{12}u_{2,i-1}\big) + F_{2,i+1}\big(t_{21}u_{2,i-2} + t_{22}u_{2,i-1}\big) \\ & + F^T_{2,i+2}\big(t_{31}\bar{u}_{2,i-2} + t_{32}\bar{u}_{2,i-1}\big) + F^B_{2,i+2}\big(t_{31}\hat{u}_{2,i-2} + t_{32}\hat{u}_{2,i-1}\big)\big], \\ G_{II} = \frac{1}{2\Delta a}\big[& F_{1,i}\big(t_{11}u_{1,i-2} + t_{12}u_{1,i-1}\big) + F_{1,i+1}\big(t_{21}u_{1,i-2} + t_{22}u_{1,i-1}\big) \\ & + F^T_{1,i+2}\big(t_{31}\bar{u}_{1,i-2} + t_{32}\bar{u}_{1,i-1}\big) + F^B_{1,i+2}\big(t_{31}\hat{u}_{1,i-2} + t_{32}\hat{u}_{1,i-1}\big)\big], \end{aligned}$$

where the first subscript in the nodal force F and displacement u refer to the Cartesian coordinate and the second subscript refers to the nodal point. The parameters t_{kl} ($k = 1, 2, 3$; $l = 1, 2$) are given in [Kim and Paulino 2002]. Δa is the characteristic length of an element. The superscripts T and B indicate the regions above and below the x_1 axis, and F^T and F^B indicate the forces at top and bottom surfaces. The displacements $\bar{u}$ and $\hat{u}$ represent the relative displacement of the top and bottom parts from the crack tip.

The stress intensity factors can then be computed from the relations [Kim and Paulino 2002]:

$$K_I = \sqrt{G_I \bar{E}} \qquad \text{and} \qquad K_{II} = \sqrt{G_{II} \bar{E}},$$

where the effective Young's modulus $\bar{E}$ for an interfacial crack is defined [Suo and Hutchinson 1989] as

$$\bar{E} = 2\cosh^2(\pi\varepsilon) \Big/ \left(\frac{1}{E_1} + \frac{1}{E_2} \right), \text{ for plane stress,}$$
$$\bar{E} = 2\cosh^2(\pi\varepsilon) \Big/ \left(\frac{1-\nu_1^2}{E_1} + \frac{1-\nu_2^2}{E_2} \right), \text{ for plane strain,}$$

and the material mismatch index ε is related to the second Dundurs' material parameter β by

$$\varepsilon = \frac{1}{2\pi} \ln\left(\frac{1-\beta}{1+\beta} \right).$$

Another important parameter is mode mixity ψ, defined as [Wang and Suo 1990]

$$\psi = \tan^{-1}\left(\frac{K_{II}}{K_I} \right).$$

2.4. ***Serration profile and distribution.*** We selected a series of serration patterns to investigate the effect of shape and distribution on stress intensity factors and mode-mixity. We classify serrations by the peak density, that is, sparse or dense, and by peak shape, that is, small, sharp, or rectangular (see Figure 7). By controlling for density or shape, we can, through our simulations, see the effect of varying the other characteristic.

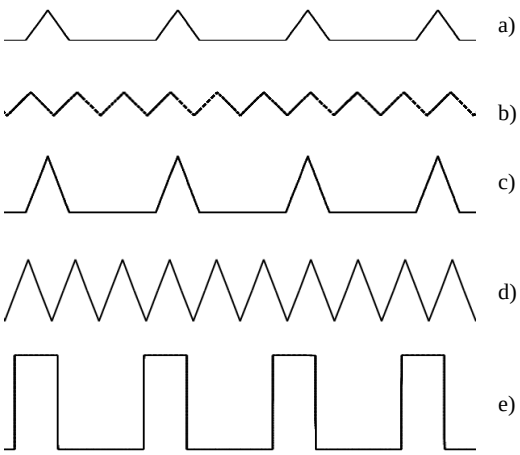

Figure 7. Serration patterns: (a) sparse small peaks; (b) dense small peaks; (c) sparse sharp peaks; (d) dense sharp peaks; (e) sparse rectangular peaks.

3. Results and discussion

For each pattern, we use FEM to find the stress intensity factor (SIF) and mode mixity. We calculated the SIF's using the virtual crack extension method [Matos et al. 1989] and summarize the results in Figures 8 through 14. We focus on how SIF magnitudes and phase angle vary along the crack, and how this variation depends on the type of serration.

Figure 8 illustrates how stress intensity factors K and mode mixity ψ vary in the presence of small sparse peaks (peak angle 45.0°) and, for comparison, in the absence of any serration. Between peaks, introducing the serrated edge slightly modifies K and ψ. However, directly above the peaks, they change substantially due to local effects. A sparse small serration evidently has only a localized effect on K and ψ.

Figure 9 illustrates the same, but with denser peaks (peak angle still 45.0°). Introducing this serration causes a dramatic undulation of K_1 and ψ. However, K_2 substantially decreases, meaning that sliding is restrained at the interface.

In Figure 10, we consider sparse, but somewhat sharper peaks (peak angle 63.4°). This causes slight change of K and ψ between the peaks, but, directly at the peaks, K and ψ change more than they did for smaller peaks.

In Figure 11, we make the previous peaks more dense. In comparison with Figure 9, we see an even greater undulation of K and ψ.

Next, in Figure 12 and Figure 13, we consider sharp, sparse peaks with peak angles 76.0° and 80.5°. As expected, sharpening the peaks continues to magnify the change in K and ψ in their vicinity, while the values elsewhere remain relatively fixed.

Table 2 summarizes the effects of sparse serration as the peaks vary from small to sharp, that is, as the angle increases from 45.0°–80.5°. Although sparse serration has only a local effect near the peaks, the effect increases as the angle increases.

Figure 14 illustrates the effect of sparse rectangular peaks. The rectangular peaks effect substantially the nearby interfacial fracture, and there is also a transition from global mode I to local mode II.

	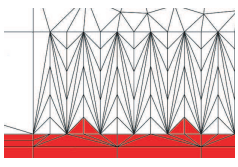	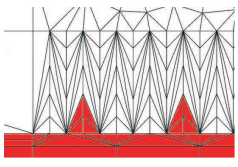	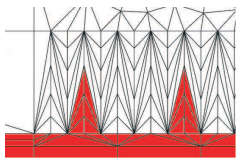	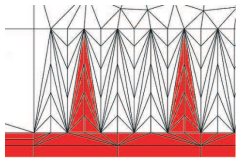
Angle (°)	45.0	63.4	76.0	80.5
Norm K_1	1.63	1.66	1.42	1.31
Norm K_2	0.01	−1.00	− 1.22	−1.33
ψ(°)	0.2	−18.7	−25.8	29.4

Table 2. Comparison of sparse serration from small to sharp.

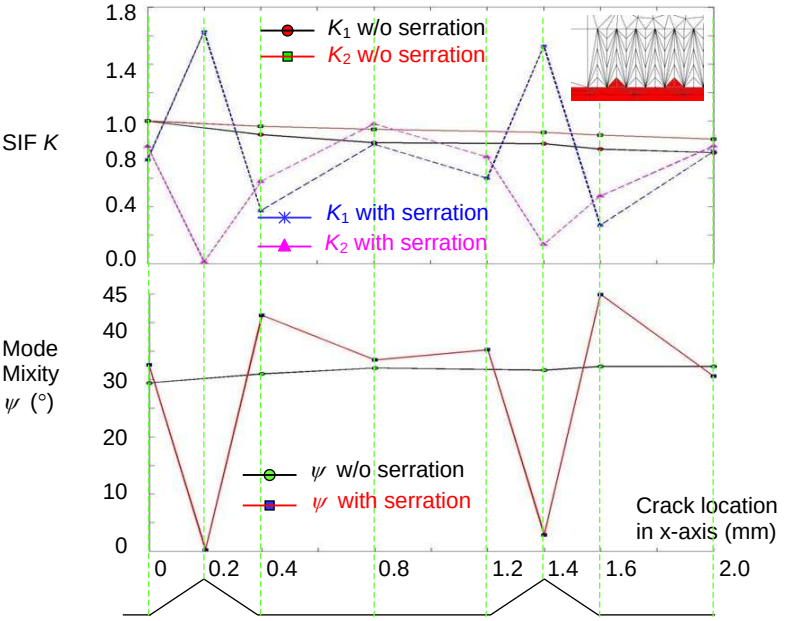

Figure 8. K and ψ versus crack location for sparse small serrations (45.0°).

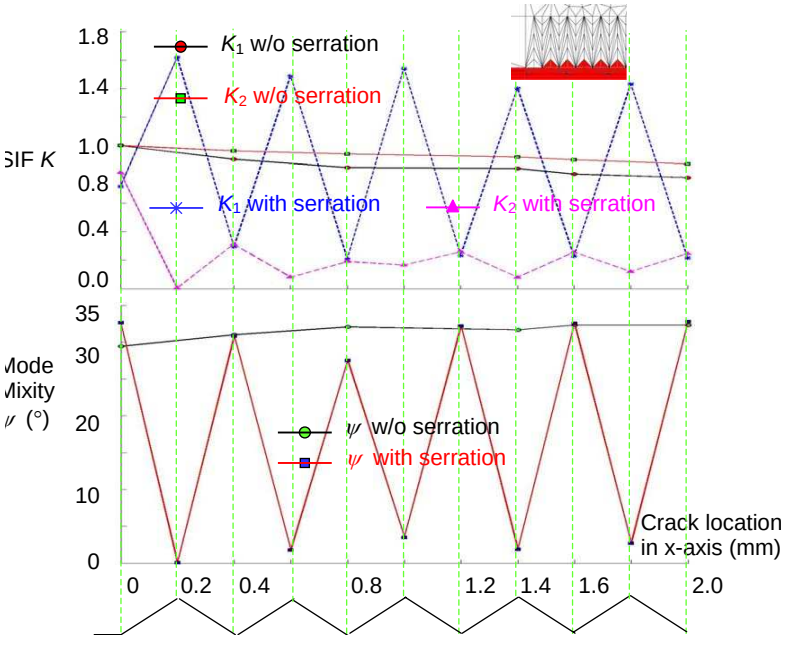

Figure 9. K and ψ versus crack location for dense small serrations (45.0°).

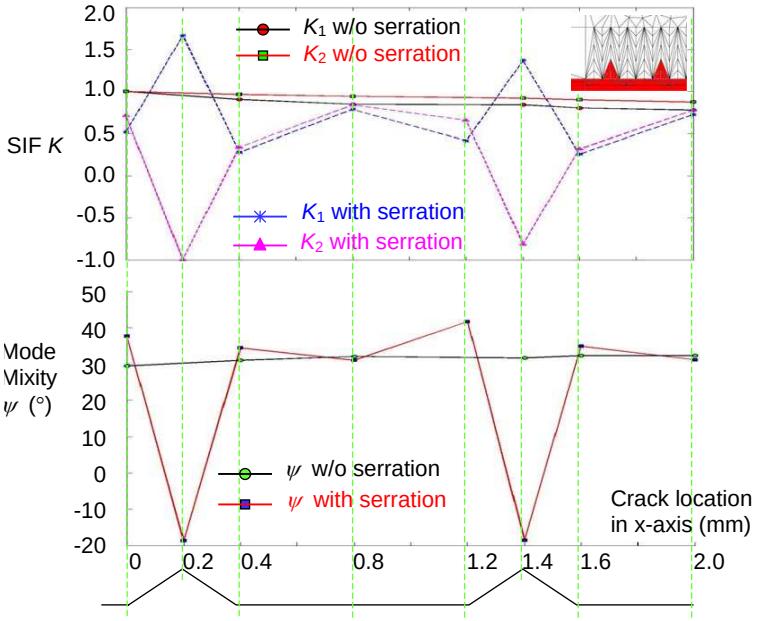

Figure 10. K and ψ vs crack location for sparse medium serrations (63.4°).

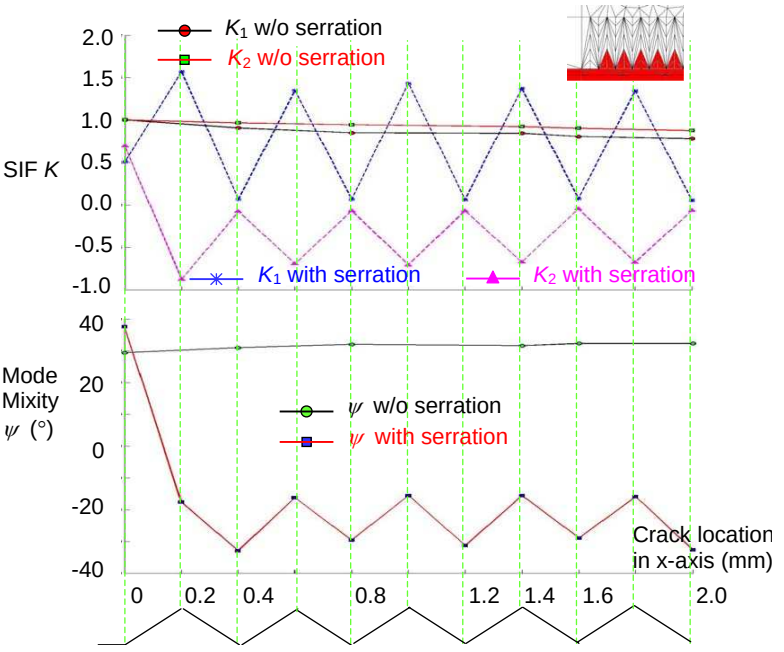

Figure 11. K and ψ vs crack location for dense medium serrations (63.4°).

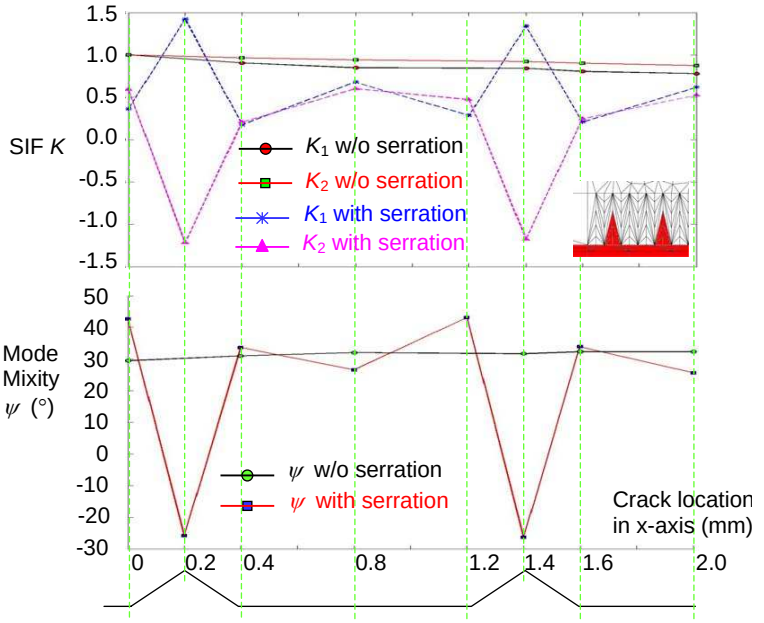

Figure 12. K and ψ vs crack location for sparse sharp serrations (76.0°).

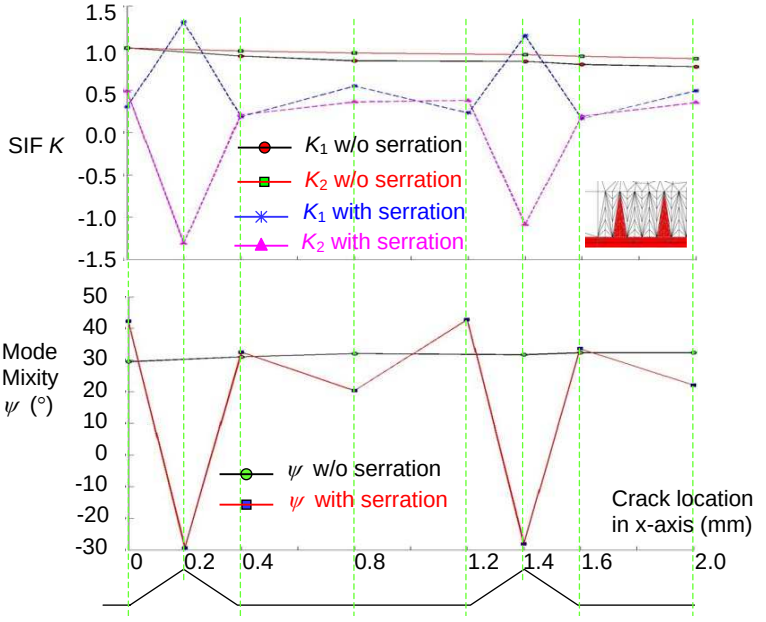

Figure 13. K and ψ vs crack location for sparse sharp serrations (80.5°).

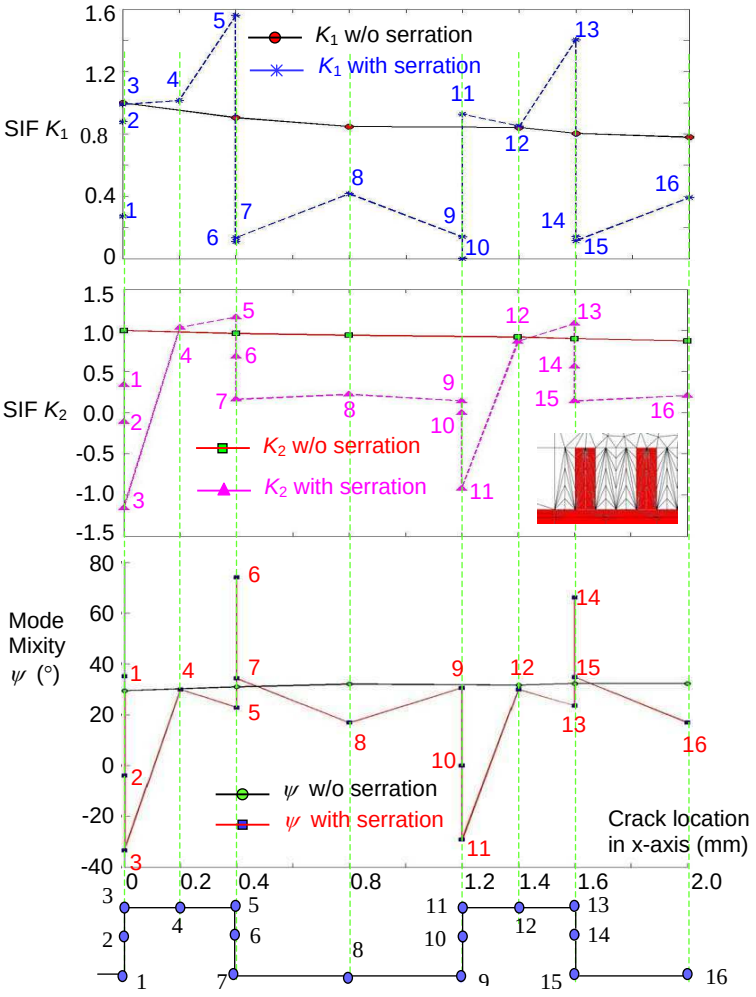

Figure 14. K and ψ vs crack location for sparse rectangular serrations (90.0°).

4. Conclusions

From our simulation and analysis, we conclude the following. (i) Sparse serration affects interfacial fracture only locally, near the serration's peaks. By sharpening the peaks, we demonstrate the effect of geometry: the disruption increases with peak sharpness. (ii) By making the peaks more dense, we study the effect of distribution: dense serration causes an undulation of the stress intensity factor and mode mixity along the interface. (iii) Altogether different geometry, namely rectangular peaks, can cause a transition from a global opening load (mode I) to a local shearing load (mode II).

Acknowledgements

This work was sponsored by the National Science Foundation, Career Award CMS-9982023. The authors gratefully acknowledge this financial support and are thankful to the Program Manager, Dr. Jorn Larsen-Basse for his genuine interest and encouragement.

References

[Cao and Evans 1989] H. C. Cao and A. G. Evans, "An experimental study of the fracture resistance of bimaterial interfaces", *Mech. Mater.* **7**:4 (1989), 295–304.

[Diao and Kandori 2006] D. Diao and A. Kandori, "Finite element analysis of the effect of interfacial roughness and adhesion strength on the local delamination of hard coating under sliding contact", *Tribol. Int.* **39**:9 (2006), 849–855.

[Diao and Kato 1994] D. Diao and K. Kato, "Interface yield map of a hard coating under sliding contact", *Thin Solid Films* **245** (1994), 115–121.

[Gilchrist and Svensson 1995] M. D. Gilchrist and N. Svensson, "A fractographic analysis of delamination within multidirectional carbon/epoxy laminates", *Compos. Sci. Technol.* **55**:2 (1995), 195–207.

[Gilchrist et al. 1996] M. D. Gilchrist, A. J. Kinloch, and F. L. Matthews, "Mechanical performance of carbon-fibre and glass-fibre-reinforced epoxy I-beams: II. fractographic failure observation", *Compos. Sci. Technol.* **56**:9 (1996), 1031–1045.

[Hutchinson and Suo 1992] J. W. Hutchinson and Z. Suo, "Mixed mode cracking in layered materials", *Adv. Appl. Mech.* **29** (1992), 63–187.

[Kim and Paulino 2002] J.-H. Kim and G. H. Paulino, "Finite element evaluation of mixed mode stress intensity factors in functionally graded materials", *Int. J. Numer. Meth. Eng.* **53**:8 (2002), 1903–1935.

[La Saponara et al. 2002] V. La Saponara, H. Muliana, R. Haj-Ali, and G. A. Kardomateas, "Experimental and numerical analysis of delamination growth in double cantilever laminated beams", *Eng. Fract. Mech.* **69**:6 (2002), 687–699.

[Larson and Miles 1998] M. C. Larson and H. F. Miles, "On the effects of friction, roughness and toughness on interfacial sliding in brittle composites", *Mech. Mater.* **27**:2 (1998), 77–89.

[Lee and Qu 2003] H.-Y. Lee and J. Qu, "Microstructure, adhesion strength and failure path at a polymer/roughened metal interface", *J. Adhes. Sci. Technol.* **17**:2 (2003), 195–215.

[Liechti 2007] K. M. Liechti, *Interfacial crack growth at glass epoxy interfaces*, 2007. Research described at author's website www.ae.utexas.edu/research/mssm/KML_BIO.htm.

[Lucksanasombool et al. 2003] P. Lucksanasombool, W. A. Higgs, R. J. Higgs, and M. Swain, "Interfacial fracture toughness between bovine cortical bone and cements", *Biomaterials* **24**:7 (2003), 1159–1166.

[Matos et al. 1989] P. P. L. Matos, R. M. McMeeking, P. G. Charalambides, and M. D. Drory, "A method for calculating stress intensities in bimaterial fracture", *Int. J. Fracture* **40**:4 (1989), 235–254.

[Mishnaevsky and Gross 2005] L. L. Mishnaevsky and D. Gross, "Deformation and failure in thin films/substrate systems: methods of theoretical analysis", *Appl. Mech. Rev.* (*Trans.ASME*) **58**:5 (2005), 338–353.

[Narayana and Dattaguru 1996] K. B. Narayana and B. Dattaguru, "Certain aspects related to computation by modified crack closure integral (MCCI)", *Eng. Fract. Mech.* **55**:2 (1996), 335–339.

[Packham 2003] D. E. Packham, "Surface energy, surface topography and adhesion", *Int. J. Adhes. Adhes.* **23**:6 (2003), 437–448.

[Partridge and Singh 1995] I. K. Partridge and S. Singh, "Mixed-mode fracture in an interleaved carbon-fibre/epoxy composite", *Compos. Sci. Technol.* **55**:4 (1995), 319–327.

[Raju 1987] I. S. Raju, "Calculation of strain-energy release rates with higher order and singular finite elements", *Eng. Fract. Mech.* **28**:3 (1987), 251–274.

[Ramulu et al. 2001] M. Ramulu, G. Paul, and J. Patel, "EDM surface effects on the fatigue strength of a 15 vol% SiCp/Al metal matric composite material", *Compos. Struct.* **54**:1 (2001), 79–86.

[Rybicki and Kanninen 1977] E. F. Rybicki and M. F. Kanninen, "A finite element calculation of stress intensity factors by a modified crack closure integral", *Eng. Fract. Mech.* **9**:4 (1977), 931–938.

[Schuller et al. 1999] T. Schuller, W. Beckert, and B. Lauke, "A finite element model to include interfacial roughness into simulations of micromechanical tests", *Comp. Mater. Sci.* **15**:3 (1999), 357–366.

[Sethuraman and Maiti 1988] R. Sethuraman and S. K. Maiti, "Finite element based computation of strain energy release rate by modified crack closure integral", *Eng. Fract. Mech.* **30**:2 (1988), 227–231.

[Straffelini 2001] G. Straffelini, "A simplified approach to the adhesive theory of friction", *Wear* **249**:1-2 (2001), 78–84.

[Suo and Hutchinson 1989] Z. Suo and J. W. Hutchinson, "Sandwich test specimens for measuring interface crack toughness", *Mater. Sci. Eng.* **107** (1989), 135–143.

[Swenson and James 1997] D. Swenson and M. James, "FRANC2D/L: a crack propagation simulator for plane layered structures", 1997, Available at http://www.fim.utp.ac.pa/FTP/Linux/CASCA/Short.pdf. Short user's guide. Version 1.4.

[Wang and Agrawal 2000] X. Wang and C. M. Agrawal, "A mixed mode fracture toughness test of bone-biomaterial interface", *J. Biomed. Mater. Res.* **53**:6 (2000), 664–672.

[Wang and Suo 1990] J.-S. Wang and Z. Suo, "Experimental determination of interfacial toughness curves using Brazil-nut-sandwiches", *Acta Metall. Mater.* **38**:7 (1990), 1279–1290.

[Young 2001] L.-J. Young, "A further investigation of mixed mode loading center crack problem", *Int. J. Solids Struct.* **38**:42-43 (2001), 7461–7471.

Received 4 Jan 2007. Accepted 31 May 2007.

ASSIMINA A. PELEGRI: pelegri@jove.rutgers.edu
Mechanical and Aerospace Engineering, School of Engineering, Rutgers, The State University of New Jersey, 98 Brett Road, Piscataway, NJ 08854-8058, United States

BAOXIANG X. SHAN: bxshan@eden.rutgers.edu
Mechanical and Aerospace Engineering, School of Engineering, Rutgers, The State University of New Jersey, 98 Brett Road, Piscataway, NJ 08854-8058, United States